Time Resolved Divergence Mapping and Long Duration Emission Studies of an Ionic Liquid Ferrofluid Electrospray Source

IEPC-2017-109

Presented at the 35th International Electric Propulsion Conference
Georgia Institute of Technology • Atlanta, Georgia • USA
October 8 – 12, 2017

Brandon A. Jackson[1] and Lyon B. King[2]
Michigan Technological University, Houghton, MI, 49931, USA

Abstract: The electrospray emission of a super-paramagnetic fluid in the presence of a strong magnetic field is investigated herein. Magnetic particles within the spray fluid experience a Kelvin force while electrically charged particles transiting the magnetic field are subject to a *qv*×*B* term in the Lorentz force. A numerical study was conducted to simulate the trajectories of electrosprayed particles influenced by both of these forces. It was found that the free-space trajectory displacement from both Kelvin and Lorentz forces was insignificant in comparison to the strong electrostatic forces. Long duration emission (6-8 hours) was then observed experimentally for two different conditions: a nominally 300-Gauss magnetic field and a 515-Gauss magnetic field. During the tests angular-resolved spray divergence measurements were taken within the emission plume using a nine-pad current collector probe. The results show no systematic differences in overall plume angular divergence between the two magnetic field cases.

Nomenclature

$\vec{a}_m$	=	Lorentz Acceleration (m/s^2)
B	=	Magnetic Flux Density (T)
$\vec{E}$	=	Electric Field (V/m)
$\vec{F}_e$	=	Coulomb Force (N)
$\vec{f}_m$	=	Kelvin Force Density (N/m^3)
$\vec{F}_m$	=	Kelvin Force (N)
H	=	Magnetizing Field (A/m)
$I_\rho(\theta)$	=	Angular Current Density (A)
I_{sp}	=	Specific Impulse (s)
M	=	Magnetization (A/m)
M_d	=	Saturation Magnetization (A/m)
m	=	Particle/Ion Mass (kg)
q	=	Particle/Ion Charge (C)
Q_r	=	Rayleigh Charge Limit (C)
T_{ideal}	=	Idealized Thrust (N)
V	=	Electric Potential (V)
$\bar{V}$	=	Droplet Volume (m^3)
γ	=	Surface Tension (N/m^2)
ε_0	=	Permittivity of Free Space (F/m)
η	=	Coulomb/Kelvin Force Ratio
μ_r	=	Relative Permeability
ρ	=	Fluid Density (kg/m^3)
χ_m	=	Magnetic Susceptibility

[1] Graduate Research Assistant, Mechanical Engineering-Engineering Mechanics, bajackso@mtu.edu.
[2] Professor, Mechanical Engineering-Engineering Mechanics, and lbking@mtu.edu.

I.Introduction

THIS paper presents two studies on the electrospray of ionic liquid ferrofluid (ILFF). Ionic liquid ferrofluids are electrically conductive super-paramagnetic fluids which respond strongly in the presence of electric and magnetic fields. When a small reservoir of ILFF is positioned within a magnetic field, magnetic stresses will deform the fluid interface into a peak. The addition of a strong electric field will further stress the fluid interface until a threshold stress is reached at which point the surface tension cannot contain the combined stresses and a spray of fluid or ions results at the apex. This process, described in more detail in Figure 1, is termed electrospray, albeit a less understood form of electrospray owing to the addition of magnetic stresses which are not present in traditional electrospray. An emitting ILFF peak is presented in Figure 2.

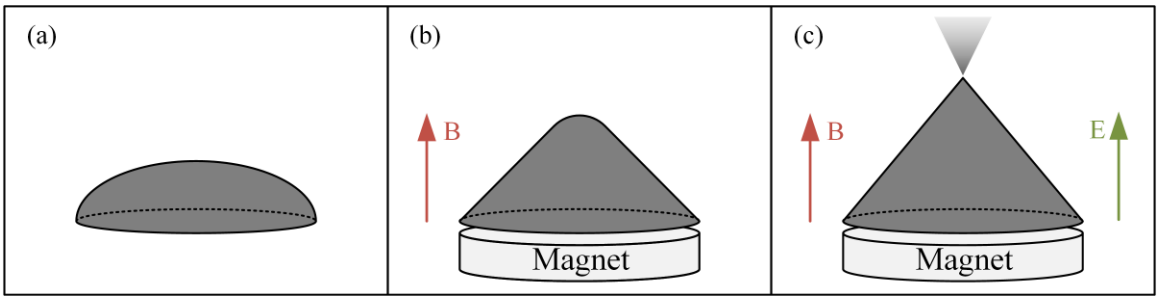

Figure 1: Electrospray emission from a combined ferro-electrohyrodynamic instability: (a) In the absence of an applied field, a sessile drop of ILFF spreads. (b) The application of a magnetic field stresses the fluid interface resulting in the fluid rising into a peak. (c) Finally, the addition of a strong electric field further stresses the fluid interface until emission results. The onset potential required for the combined ferro-electrohydrodynamic instability than the potential required to emit from configuration (a) as a result of the preconditioning provided by the magnetic stresses isolated in (b).

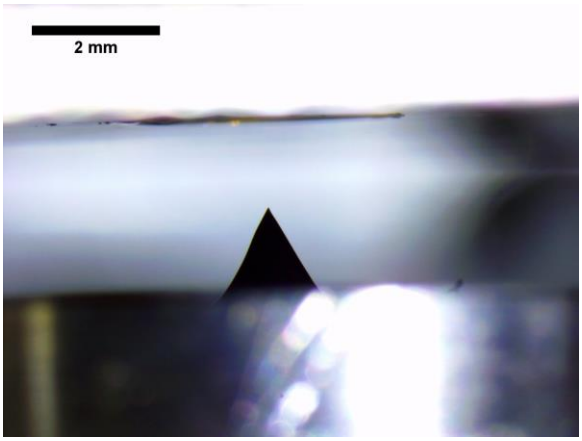

Figure 2: Electrospray emission from an emitting peak formed using a combined magneto-electric instability.

Electrospray form ferrofluids was first demonstrated by Meyer and King[2, 5, 6] in 2012. In 2014, Terhune et. al presented the first species measurement of a normal-field based emission source using a time-of-flight mass spectrometer.[7] In 2017, the authors published on a model capable of simulating the fluid interface and quantifying the magnetic and electric stress components during the leadup to emission.[8]

The ferrofluid utilized for the research presented herein was an EMIM-NTf2 ionic-liquid-based polymer-stabilized ILFF produced by the *Key Centre for Polymers and Colloids* at the University of Sydney.[3] The ferrofluid properties, presented in Table 1, maintain the desirable electrical properties of the carrier fluid while becoming super paramagnetic. The Langevin parameters β and τ relate the relative magnetic permeability of the fluid μ_r to the magnetizing field H. To obtain these parameters, a Langevin fit is performed on the magnetization curve relating the fluid magnetization M to the H field strength.

$$\mu_r = 1 + \frac{\beta}{H}\left[\coth\left(\tau|H|\right) - \frac{1}{\tau|H|}\right] \tag{1}$$

The first study included in this paper presents a numerical model to quantify the magnitude of the Kelvin and Lorentz force on emitted particles. Kelvin forces are predicted by solving for the gradient in the magnetic field and electric potential near the apex of a modeled Taylor cone. The Kelvin force is presented as a ratio to the coulomb force in the same region. The second study presents an approach to obtaining time-resolved angular divergence measurements of ILFF electrospray along with comments on emission behavior of the source.

Table 1: Ferrofluid fluid and magnetic properties

		EMIM-NTf2 ILFF[1-4]
Density (g/cm^3)		1.815
Viscosity (mPa·s)		120
Surface Tension (mN/m)		32.389
Carrier Fluid		EMIM-NTf2
Conductivity (S/m)		0.63 S/m
Percent Solids (w/w)		17.3, 20.6
Particle Size		~10-12 nm
Langevin Fit	β (A/m)	2.335 x 10^4
	τ (m/A)	2.408 x 10^{-4}
	R^2	0.959

II.Estimating Forces on an Emitted Particle

Near the apex of an emitting Taylor cone, the electric field is very intense with strong radial components. In the case of ion evaporation, the electric field near the apex can be in the range of $1x10^9$ V/m.[9] In this region, the considerably strong radial components of the electric field is a leading factor in the spray divergence of an electrospray source. The objective of this short study was to analyze the influence of the Kelvin force and Lorentz force on droplets resulting from electrospray emission in the proximity of the Taylor cone apex. The goal is to approximate the relative magnitude of the Kelvin, Coulomb, and Lorenz forces to determine their contribution to the particle motion. The analysis presented herein makes a considerable number of assumptions whose effect will be discussed individually in Section II.C.

A. Kelvin Force Analysis

The small size of the emitted droplets allows each droplet to be modeled as a magnetic dipole. The Kelvin force density acting on a dipole within a magnetic field is:[10]

$$\vec{f}_m = \mu_0\left(\vec{M}\cdot\vec{\nabla}\right)\vec{H}_0 \tag{2}$$

Where $\vec{f}_m$ is the Kelvin magnetic force density in force per unit volume, $\vec{M}$ is droplet magnetization, and $\vec{H}_0$ is the magnetic field strength of the free field, i.e., the magnetic field at the location of the droplet while neglecting the field contributions from the droplet. Expanding Eq. (2) in cylindrical coordinates yields:

$$\vec{f}_m = \frac{d\vec{v}}{dt} = \mu_0\left[\left(M_r\frac{\partial H_{0r}}{\partial r} + M_z\frac{\partial H_{0r}}{\partial z}\right)\hat{r} + \left(M_r\frac{\partial H_{0z}}{\partial r} + M_z\frac{\partial H_{0z}}{\partial z}\right)\hat{z}\right] \tag{3}$$

The Rayleigh limit expresses the maximum charge a stable droplet can contain.[11] Above this limit, the droplet becomes unstable and will disintegrate into smaller droplets. This limit is given as:

$$Q_r = 2\pi\left(16\pi^2\varepsilon_0\gamma r^3\right)^{1/2} \tag{4}$$

where Q_r is the Rayleigh charge limit. Not all electrospray droplets are charged to the full Rayleigh limit. The parameter $\Phi \in (0,1)$ denotes the Rayleigh limit charge factor. A value of $\Phi = 0.5$ will be assumed here to present a reasonable value of droplet charge. The Coulomb force on a droplet becomes:

$$\vec{F}_e = \Phi Q_r\vec{E} \tag{5}$$

The Coulomb/Kelvin force ratio becomes:

$$\eta = \frac{\vec{F}_e}{\vec{F}_m} = \frac{\left|\Phi Q_r \vec{E}\right|}{\left|\bar{V}\mu_0\left(\vec{M}\cdot\vec{\nabla}\right)\vec{H}_0\right|} \tag{6}$$

where $\bar{V}$ is the droplet volume.

B. Modeling Approach

To obtain a representative comparison of the ratio of Coulomb to Kelvin force in ferrofluid electrospray, two particles will be analyzed. Coulomb forces will be calculated for a 30 nm spherical fluid droplet charged to 50% of the Rayleigh limit, $\Phi = 0.5$. Kelvin forces will be calculated for a 30 nm radius spherical single-domain iron oxide particle at the material saturation magnetization for magnetite, which is 4.45x10^5 A/m.[10] The geometric domain utilized for this study is based on the emitter apparatus which will be presented in Section III.B.

1. Taylor Cone Model

A static model was implemented to model the fluid interface based on pervious work published by Krpoun and Shea.[12] Their approach implemented a Bernstein-Bézier curve to model the fluid interface. Although this model is non-physical, i.e., the interface stresses do not balance perfectly, it makes an accurate representation of the Taylor cone geometry. Krpoun and Shea implemented this interface model to computationally predict the onset voltage of a traditional electrospray source. In Cartesian coordinates, the surface is expressed as:

$$x(t,w,\phi) = \frac{(1-2t)\,p_x}{1-2t(1-t)(1-w)}\cos(\phi) \tag{7}$$

$$z(t,w,\phi) = \frac{2(1-t)tw\cot(\beta)\,p_x}{1-2t(1-t)(1-w)} \tag{8}$$

where the Taylor cone half angle, β, is 49.3° and p_x is the base radius of the Taylor cone. In the XZ plane, the angular coordinate $\phi = 0$. The apex radius is:

$$r_a = \frac{p_x}{w}\tan(\beta) \tag{9}$$

For a 1.5-mm diameter reservoir, the Bernstein-Bézier model for a Taylor cone is presented in Figure 3:

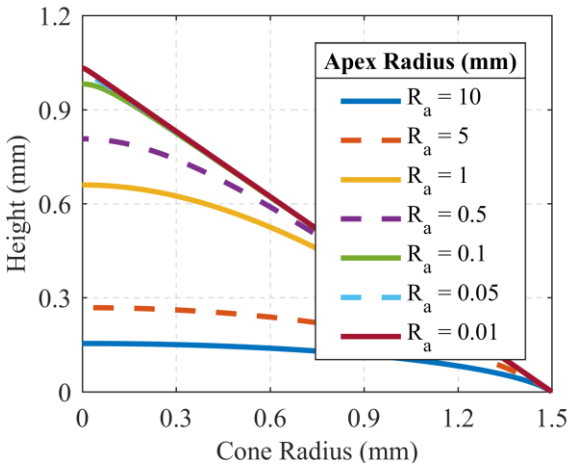

Figure 3: Bernstein-Bézier Taylor Cone model for a Taylor cone half angle of 49.3°.

2. FEA Model

The ferrofluid simulated in this study was treated as a rigid entity having the material magnetic and electrical properties of the ILFF presented in Table 1. A magnetic field was generated from the presence of two 1" dia. x 1/8" thick N42 disk magnets. The magnets were modeled with a residual induction, Br_{max}, of 13,000 Gauss with a relative permeability, μ_r, of 1.05. The resulting field at the reservoir interface in the absence of ferrofluid was 520 Gauss at the top surface of the fluid reservoir. The actual field for the emitter in this configuration was measured to be 515 Gauss.

The interface equations, presented in Eqs. (7) and (8), were utilized to model the fluid geometry above the reservoir. The apex radius was set to 1 μm, yielding an apex electric field of $6x10^7$ V/m. The computational domain is presented in Figure 4. The fluid interface was partitioned into separate domains near the fluid apex. This enabled the region where the highest gradient exists to be meshed independently, allowing fine control over the mesh in this region. Quartic elements were selected to solve for the magnetic and electric scalar potential. A mesh refinement study was performed in which the concentration of elements in the apex region was increased and decreased by a factor of 2.5. No difference was observed in the first four significant figures of either the magnetic or electric fields.

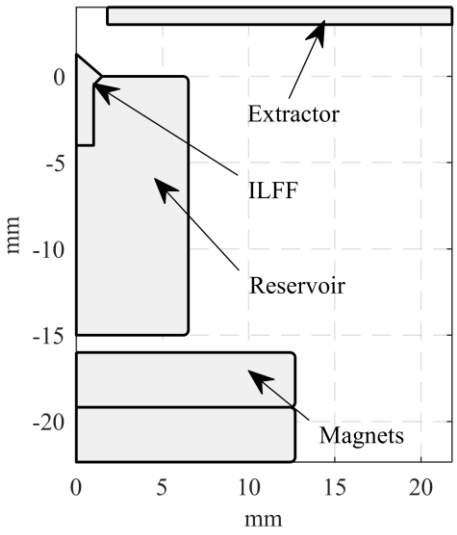

Figure 4: Subset of computational domain for FEA. Computational domain was axisymmetric around the y-axis.

C. Kelvin Force Modeling Results

The electric potential, electric field magnitude, magnetic field magnitude along with the force ratio comparison are presented in the following figures.

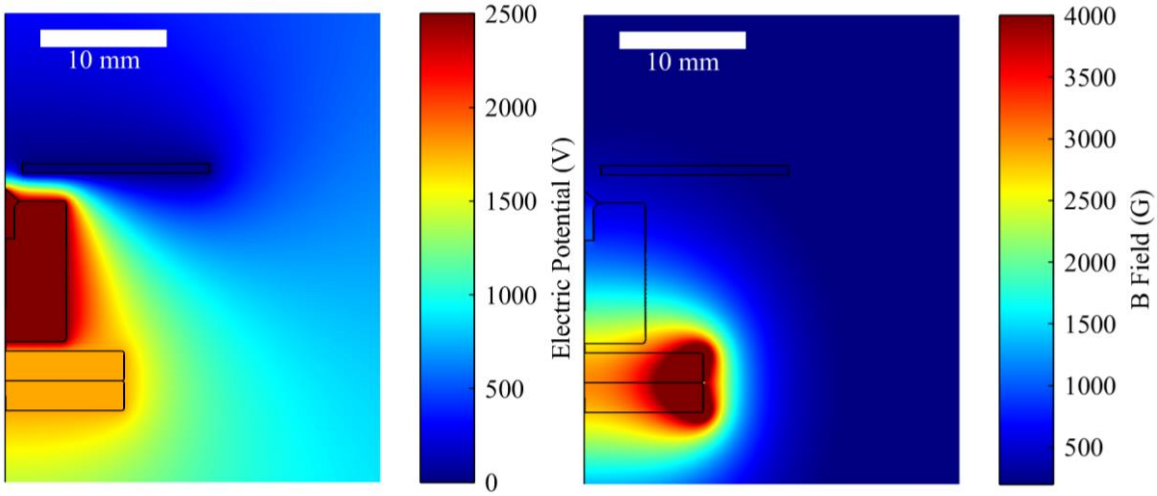

Figure 5: (Left) Electric potential for the entire emitter geometry. (Right) Magnetic field within the entire emitter geometry.

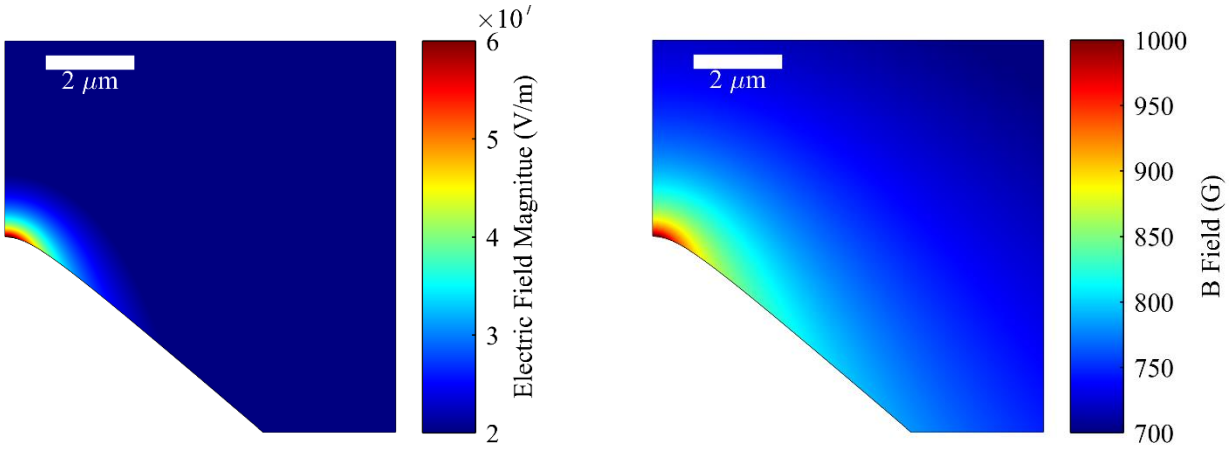

Figure 6: (Left) Electric field in the proximity of the Taylor cone apex. (Right) Magnetic field strength in in the proximity of the Taylor cone apex.

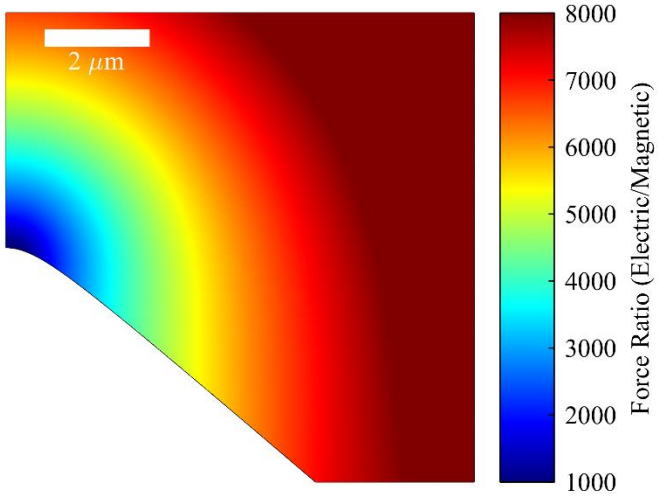

Figure 7: Electric to Kelvin force ratio near the apex of a Taylor Cone.

From Figure 7, it becomes apparent that the Kelvin force acting on a spherical 30-nm radius saturated magnetite particle is considerably smaller than an equivalent sized spherical fluid droplet at 50% of the Rayleigh limit. The Coulomb force over powers the Kelvin force by three orders of magnitude in the region immediately above the apex, where the ratio is the smallest.

This analysis does make a considerable number of assumptions. These assumptions will be addressed individually for their potential impact.

1. The Taylor cone was set to have an apex radius of 1 μm with an applied voltage of 2500 V. The resulting electric field yielded a maximum magnitude of 6×10^7 V/m at the Taylor cone apex. This is below the $\approx 1 \times 10^9$ V/m limit necessary for ion emission. Since ions emitted from the apex will not experience Kelvin forces, only the lower electric field region where droplet emission can occur was modeled.
2. Space-charge effects are not modeled. Space charge effects result when a high density of charged particles or droplets are present in the immediate region of the apex. The combined effect of these droplets reduced the electric field and the resulting Coulomb force.
3. The interface geometry was assumed to follow a Bernstein-Bézier curve. This description is based on cone model for traditional electrospray. This model does not account for magnetic forces. Previous work by the authors which dynamically modeled the fluid interface, confirms that near onset, the electric stresses dominate in the immediate proximity to the apex while the magnetic stresses dominate elsewhere.[8] Therefore,

the use of the Bernstein-Bézier to approximate the fields in the apex region is an admissible approximation in this region where electric forces dominate by orders of magnitude.

4. Droplet emission results from breakup of the fluid jet. Although the interface is modeled as a cone rather than a cone-jet. For high conductivity fluids, the jet length has been observed to be short.[13]
5. The droplet and particle size was assumed to have a radius of 30 nm. Expanding Eq. (6) by substituting the volume and Rayleigh limit terms of the radius yields:

$$\eta = \frac{\Phi 2\pi \left(16\pi^2 \varepsilon_0 \gamma r^3\right)^{1/2} \left|\vec{E}\right|}{\frac{4}{3}\pi r^3 \left|\mu_0 \left(\vec{M}\cdot\vec{\nabla}\right)\vec{H}_0\right|} \propto \frac{r^{3/2}}{r^3} \tag{10}$$

It can be observed that the Kelvin force grows with particle size at a rate of $r^{1.5}$ faster than the Coulomb force. However, the large particle sizes necessary such that Kelvin forces would become comparable are too large to be present within the ferrofluid being considered.

D. Lorentz Force Analysis

The Lorentz force is a combination of the electric and magnetic forces on a particle and is given in the following relation:

$$\vec{F} = q\vec{E} + q\vec{v}\times\vec{B} \tag{11}$$

Where $q\vec{E}$ is the electric force and $q\vec{v}\times\vec{B}$ is the magnetic force. The electric force is the component which accelerates the charged particles in traditional electrospray. The magnetic force component only emanates when a magnetic field is present.

Assuming that the electrically charged particle is accelerated up to the full electrical potential V, the velocity of the particle becomes:

$$v = \sqrt{2\frac{q}{m}V} \tag{12}$$

Consider the scenario where $\vec{v} \perp \vec{B}$ for which the resulting $q\vec{v}\times\vec{B}$ component would be the most drastic. In such a case, the particle would begin to rotate around the $\vec{B}$ vector in a circular trajectory described by the Larmor radius:

$$r_L = \frac{mv_\perp}{|q|B} \tag{13}$$

In Figure 6, it was shown that in the region directly above the apex of the Taylor cone model, the fluid magnetization approached 0.1 Tesla (1000 Gauss). Using this value for $|B|$ and an acceleration potential of 2000 V, the Larmor radius was calculated (shown in Figure 8) with respect to the range of estimated mass-to-charge ratios for ILFF electrospray measured by Terhune.[14] The results show that the Larmor radius (~1-10s of meters) is considerably large for the emitted species relative to scale of the emission source (~ 10s of millimeters) and is thus too small to be significant factor on particle trajectory.

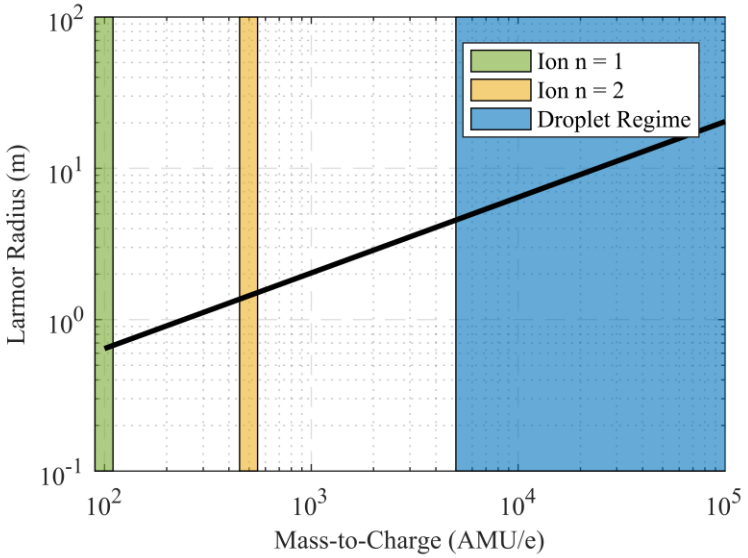

Figure 8: Larmor radius for a particle accelerated to 2000V within a 0.1T magnetic field perpendicular to the initial velocity vector.

III.Emission and Angular Divergence Studies of ILFF Electrospray

The objective of this research was to experimentally determine whether the presence of a magnetic field changes the angular divergence of an ILFF electrospray. Beam spreading materializes in the form of an off-axis beam current which originates from a near radial electric field at the fluid apex as well as space-charge effects for the case of light-ions in high emission currents.[15] Beam spreading reduces thrust efficiency for an electrospray propulsion device since off-axis particles carry non-thrust-producing momentum components. Additionally, understanding the beam divergence is critical for proper sizing of the extraction electrode orifice diameter to minimize intercepted current.

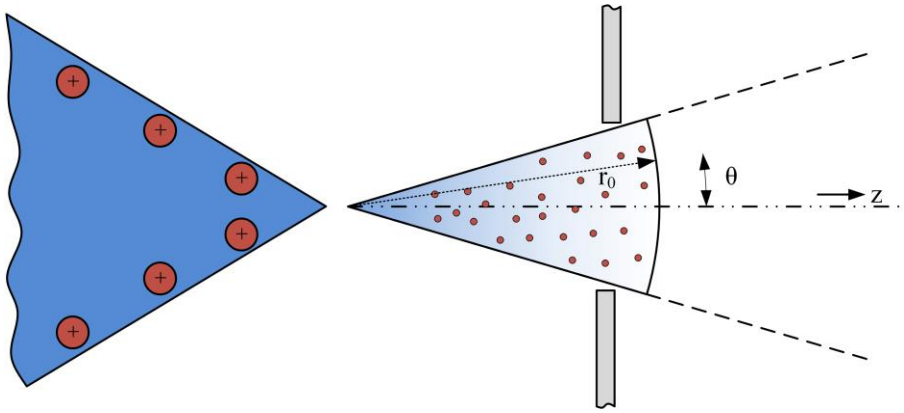

Figure 9: Beam divergence diagram.

For simplicity, consider an electrospray source, shown in Figure 9, where all emitted particles have the same mass-to-charge ratio and are emitted at the potential V_0. The emitted particles are non-collinear and can be described by an angular current density distribution $I_\rho(\theta)$ measured at location r_0. The resulting thrust provided by such an electrospray source becomes:

$$\vec{T}_{ideal} = 2\pi r_0 \left(\frac{m}{q}\right) \int_{-\pi/2}^{\pi/2} \frac{I_\rho(\theta)}{r_0} \vec{v}_e(\theta)\, d\theta \tag{14}$$

If axial symmetry exists in $I_\rho(\theta)$, Eq. (14) can be expanded as follows:

$$T_{z,ideal} = 4\pi\sqrt{2\frac{m}{q}V_0}\int_0^{\pi/2} I_\rho(\theta)\cos(\theta)d\theta \quad \hat{z} \tag{15}$$

At this point, it becomes apparent that the overall thrust provided by an electrospray source decreases with respect to a broadening of the angular current distribution. Thus, an understanding of the influential factors which control this distribution is important when developing an electrospray propulsion system.

When a super-paramagnetic fluid, like a ferrofluid, is sprayed in the presence of a magnetic field, additional factors arise which have the potential to influence the spray divergence. These factors include: (1) changes in the emission site dynamics and geometry, (2) Kelvin body force, and (3) Lorentz forces. Simulations presented in the previous chapter suggest that the Kelvin body force and Lorentz force are insignificant relative to the Coulomb force and are thus unlikely to be origin in any changes in electrospray behave within a magnetic field.

A. Previous Divergence Measuring Studies and Approaches by Other Researchers

An initial angular divergence study using ILFF was performed in the summer of 2014 by the authors.[16] In summary, this approach swept a Faraday probe in a circular profile over an ILFF emission source using a stepper motor. This approach was able to achieve excellent angular resolution. However, the method was rather slow, taking about 25 seconds for a complete sweep and thus was unable to differentiate between temporal and spatial profile variations. The limitations of this previous approach motivated the work presented herein.

Multiple approaches have been employed by various authors to obtained beam divergence measurements. Chiu et. al. and Courtney et. al. both obtained angular current distribution measurements by rotating an electrospray source and extractor electrode with respect to a measurement device.[17, 18] Gamero-Castaño obtained beam profile measurements by moving a collector plate mounted on a motion stage over an emission source.[19, 20] Spray measurements performed by Morris were obtained by a slit-shaped aperture between the extraction electrode and Faraday plate collector using a motion stage. In this method, only the spray that passed through the aperture at a given known position was measured.[21] In general, these methods achieve excellent spatial resolution but poor temporal resolution.

In 2003, Lozano presented a study which measured the angular divergence of needle-based traditional electrospray emitters.[15] The approach employed for this study consisted of a stack of 11 electrically-isolated concentric ring plates. Current was measured on each ring along various axial distances to obtain the beam spreading as a function of downstream position. This approach is capable of performing simultaneous measurements, allowing for time resolved measurements to be made of the intercepted current on each collector at the cost of decreased spatial resolution.

B. Equipment and Testing Methodologies

1. Emitter Apparatus

The electrospray emitter apparatus utilized for this study was designed by Terhune[14] with modifications in the manner in which the extractor and collector electrodes were mounted. A diagram of the emitter apparatus is presented in Figure 10:

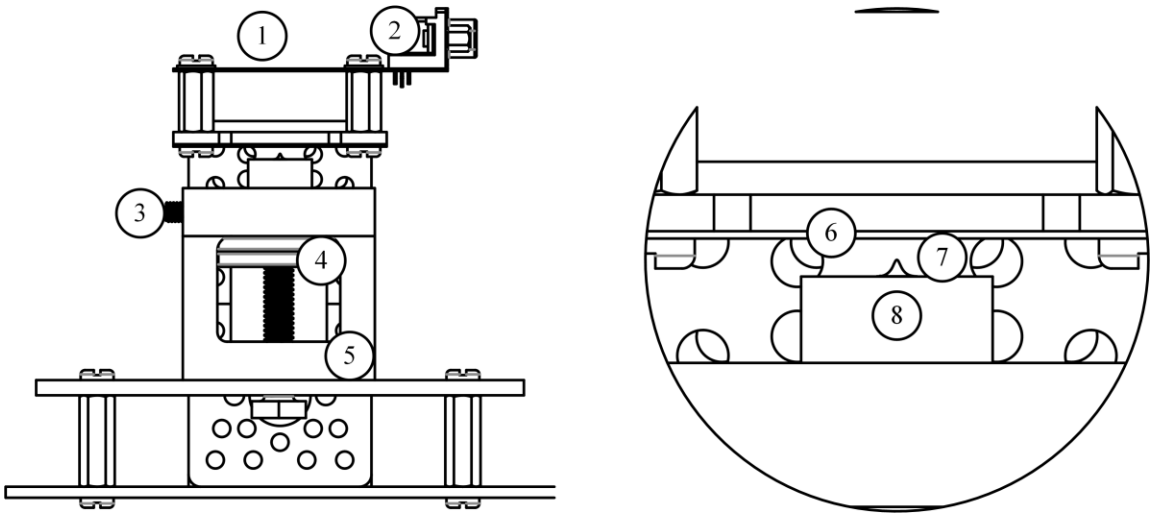

Figure 10: Electrospray emission apparatus. (1) Current collector, (2) DB-9 surface mount connector, (3) electrical bias terminal, (4), N-52 magnets, (5) PTFE isolation block, (6) Extractor electrode, (7) ferrofluid instability, and (8) fluid reservoir.

The extractor electrode was positioned 2.85 mm downstream of the fluid reservoir. The extractor and current collector were separated by 15.40 mm with an extractor thickness of 1.13 mm. When referenced to the top surface of the fluid reservoir, the probe obtained a median resolution of 4.3° between measurement locations. The reservoir was infused with 13μL of ferrofluid using a micro syringe and syringe pump. Current measurements were obtained at the emitter and collector. Intercepted current on the extractor was not measured; however, fluid buildup was never observed on the extractor during testing.

The emission source was biased with respect to the grounded extractor electrode using an Advanced Energy HVA Precision High voltage amplifier. The amplifier was controlled via a signal generator producing a 0.5 Hz square waveform. The 0.5 Hz waveform was selected since no electrochemistry of the fluid was observed at that frequency. Since fluid volume within the reservoir is depleted during testing, the extraction voltage was increased during the test with the goal of maintaining emission current between 1 and 2 μA.

2. Divergence Probe

The angularly resolved current collector probe was milled out of two-sided copper clad board. Each of the nine collector pads was routed to a pin on a board-mounted DB-9 receptacle. The milled board is shown in Figure 11. Prior to testing, each board was submerged in a 3% acetic acid solution for 30 seconds to remove any oxidation. The boards were then immediately submerged in a 95% ethyl alcohol/water solution and placed in an ultrasonic bath for 30 minutes. The collectors were then dried with a lint free cloth and placed in a vacuum to dry completely. A new board was used for each emission test.

The collected current on each of the nines segments of the probe was measured using an EEVblog μCurrent™ (original) precision current meters. These meters were operated on the 1 mV/nA scale, providing a full-scale range of ±1000 nA with a 2 kHz bandwidth.[22] Buildup of ferrofluid particles was observed on the collector during the testing. Upon completion of the test, the probe was checked for pad-to-pad continuity by biasing the center collector up to 500V and measuring the adjacent collector. The collector-to-collector resistance was typically on the order of 250MΩs,

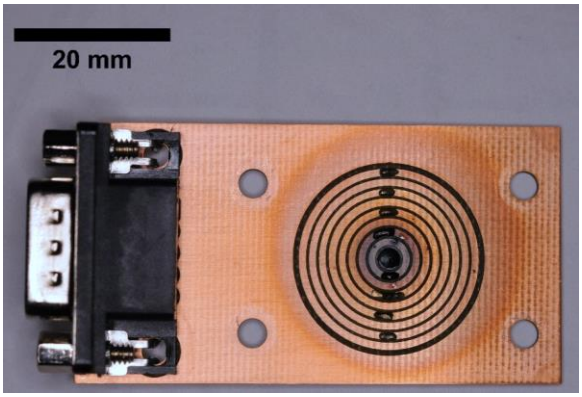

Figure 11: Current collector after approximately 6 hours of emission. Ferrofluid buildup can be observed on the center rings with decreasing intensity as the radial distance increases. Continuity between adjacent pads was tested after testing to detect pad-to-pad

indicating that the conductive film coating the surface provided a conductive, albeit small, path between adjacent collectors. Relative to the collector-to-ground resistance, the collector-to-collector path is negligible.

Close agreement was observed between emission-side current and intercepted current. Intercepted current averaged 87% of emission current. Consequently, secondary electron emission is not believed to be a considerable factor. A typical balance between emitted and intercepted current is presented in Figure 12.

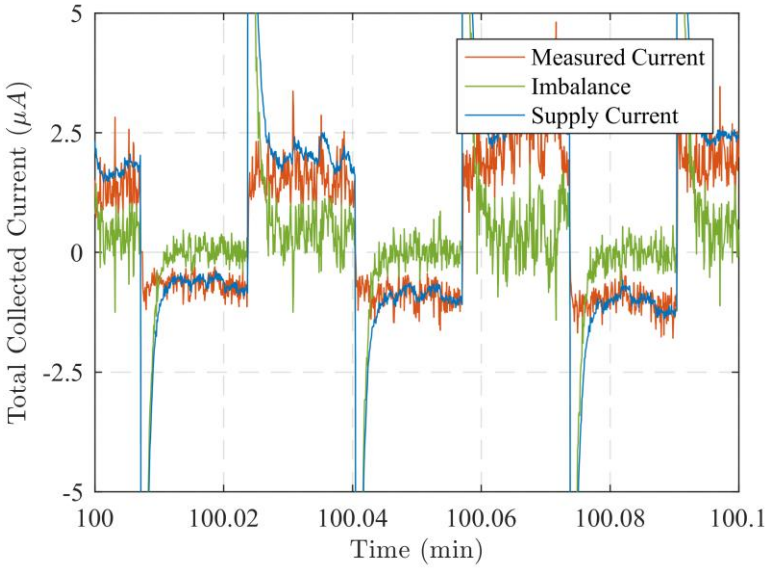

Figure 12: Typical balance between emitted and collected current. Transient spikes are present in the supply current resulting from the charging and discharging of the HV

3. Vacuum Facility and Imaging Setup

Testing was performed at vacuum within the Micropropulsion Facility-2 of the Ion Space Propulsion Laboratory at Michigan Technological University. This facility is approximately a 60-liter cylinder and is roughed down using a 300 liter/min tri-scroll pump and a 280 liter/second turbomolecular pump. The base pressure of this facility is approximately 5×10^{-7} torr. Testing was conducted when the tank pressure reached approximately 1×10^{-6}. A single emitter was found to have no measurable impact on tank pressure.

The electrospray emission apparatus was placed within a viewport in the tank—allowing for imagery to be taken of the emission source. Images were taken of the source at two-minute intervals during testing with addition images being taken during any events the authors deemed interesting. Post processing of these images allowed for an estimation to be obtained of the height of the emission source. When presenting height results, all imaged tips were normalized to the initial peak height in the presence of a magnetic field only.

C. Experimental Results

Two configurations of the emission source are presented in this section. The first, a 1-magnet configuration, had a magnetic field strength of 300 Gauss at the reservoir surface. The total collected current and extraction potential are presented in Figure 13. For this dataset, the angular divergence results for select 10-minute intervals are included in Figure 14. The second case which was considered is a 2-magnet configuration with a magnetic field strength of 515 Gauss. Results for this configuration are presented in Figure 15 and Figure 16.

In comparison, the 1- and 2-magnetic configuration demonstrated similar divergence patterns in that both cases the current fell to zero at approximately 20°.

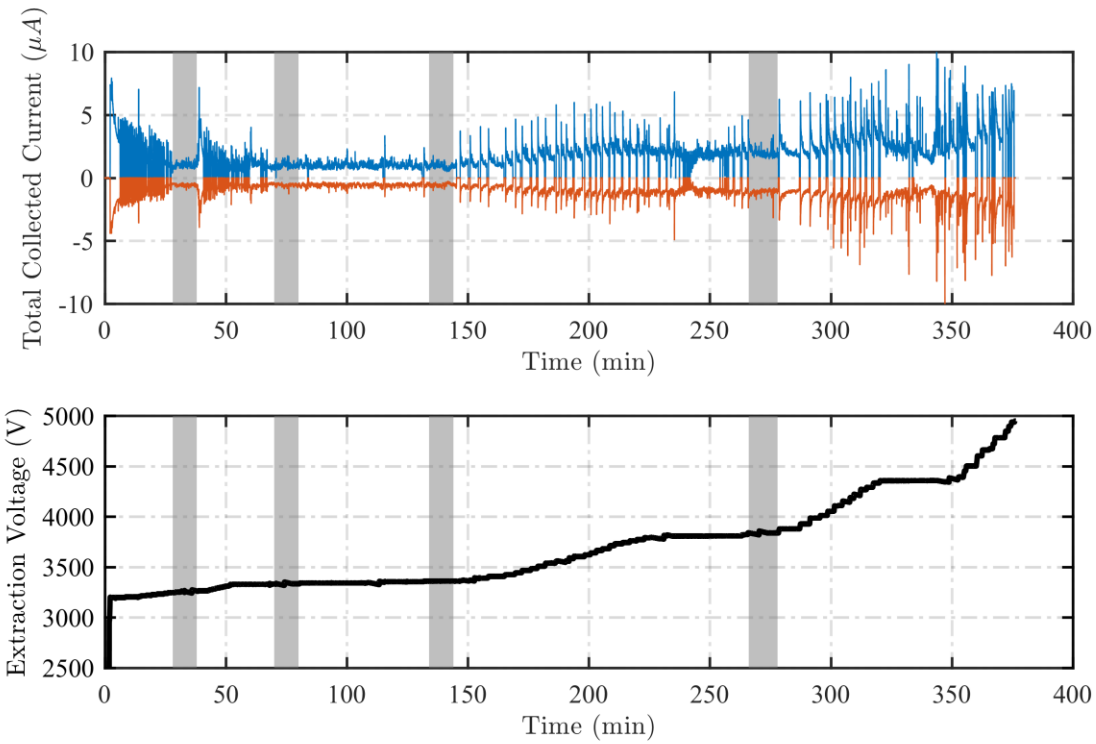

Figure 13: Long duration test in 1-magnet configuration (B=300 G). Image data was not taken for this test.

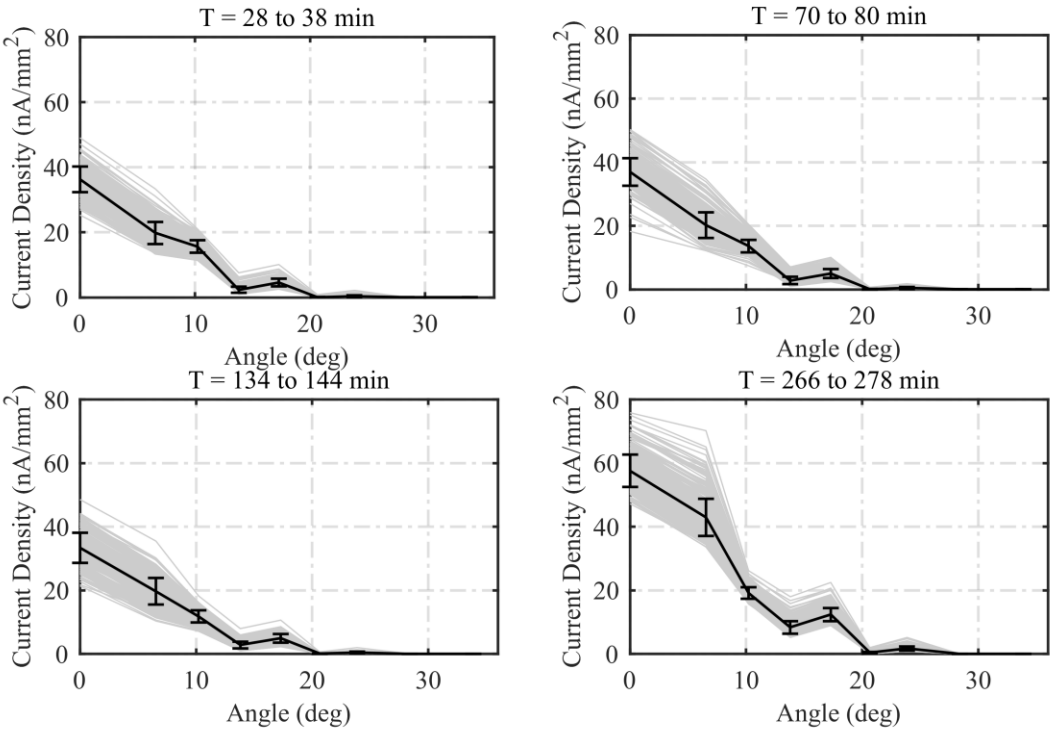

Figure 14: Divergence measurements at select 10-minute intervals during 1-magnet configuration test.

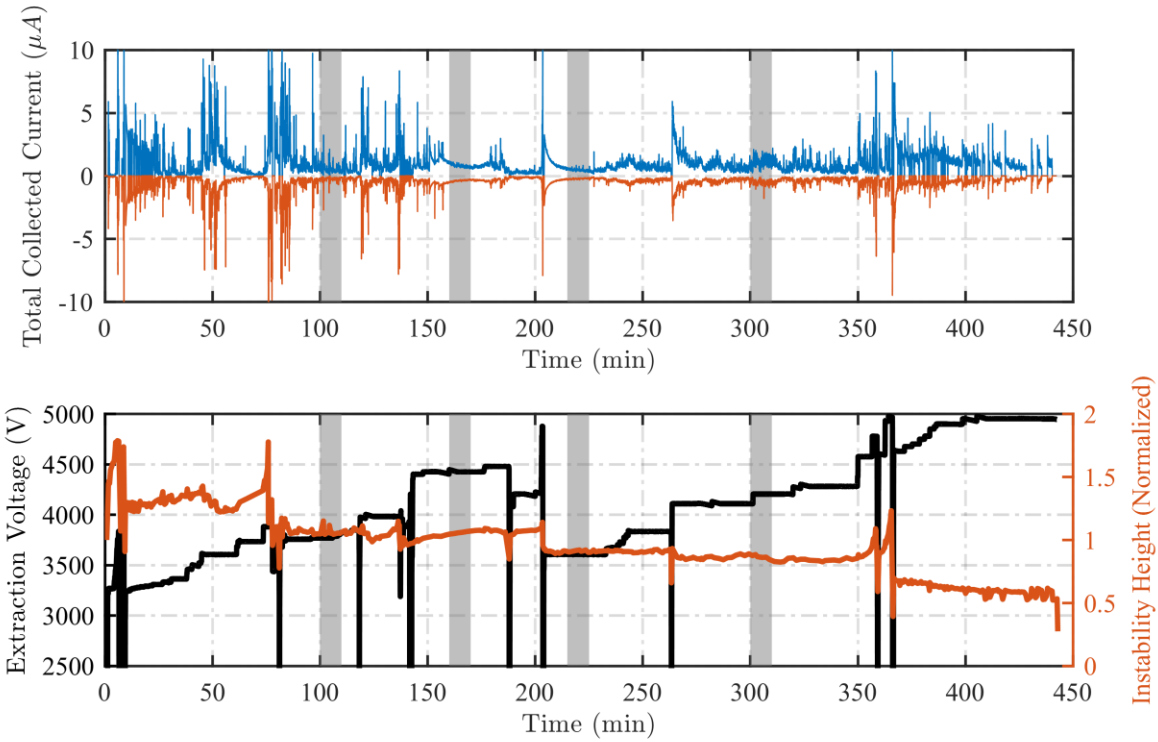

Figure 15: Long duration test in 2-magnet configuration (B=515 G).

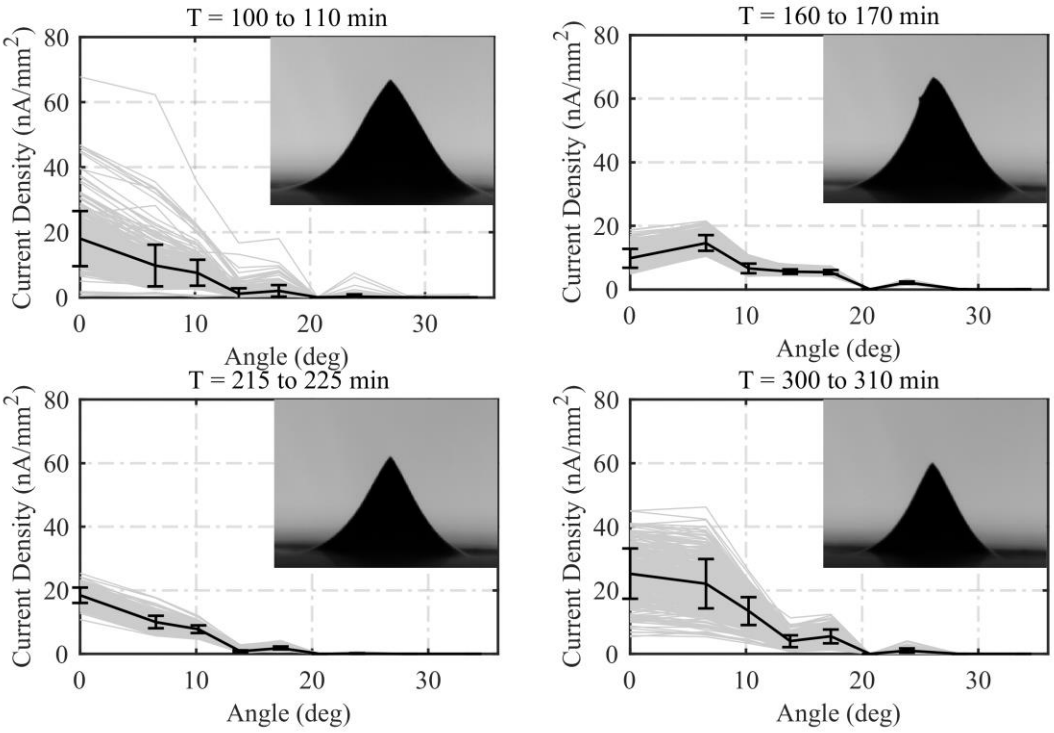

Figure 16: Divergence measurements at select 10-minute intervals during 2-magnet configuration test.

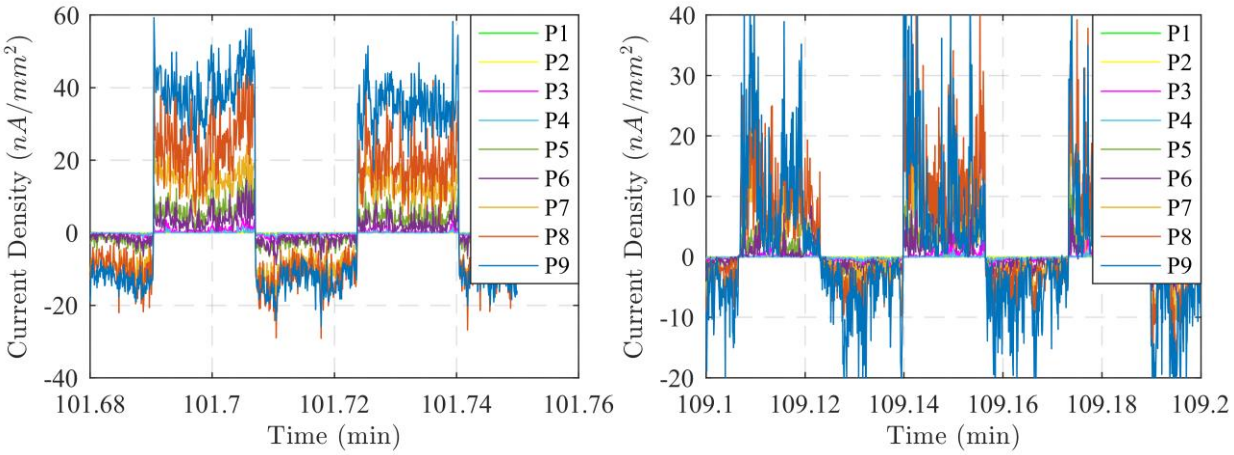

Figure 17: (Left) Typical emission current for a steady emitting Rosensweig ferrofluid electrospray source. Probes are numbered sequentially such that P1 is the outermost collector and P9 is the center collector. Emitter is in a stable emission mode with a single emission site. (Right) Typical emission current pattern for multiple emission site mode. NOTE: graphs are not from the same test.

D. Notable Phenomenon Observed During Emission

Periodically during testing, it was observed that the ferrofluid source would form a blunt apex on top of which multiple Taylor cones were observed to subsist simultaneously. During such an occasion, it was possible to maintain an emission voltage for extended durations without the self-extinguishing although higher than normal voltages to achieve onset were required. One such case is presented below in Figure 18.

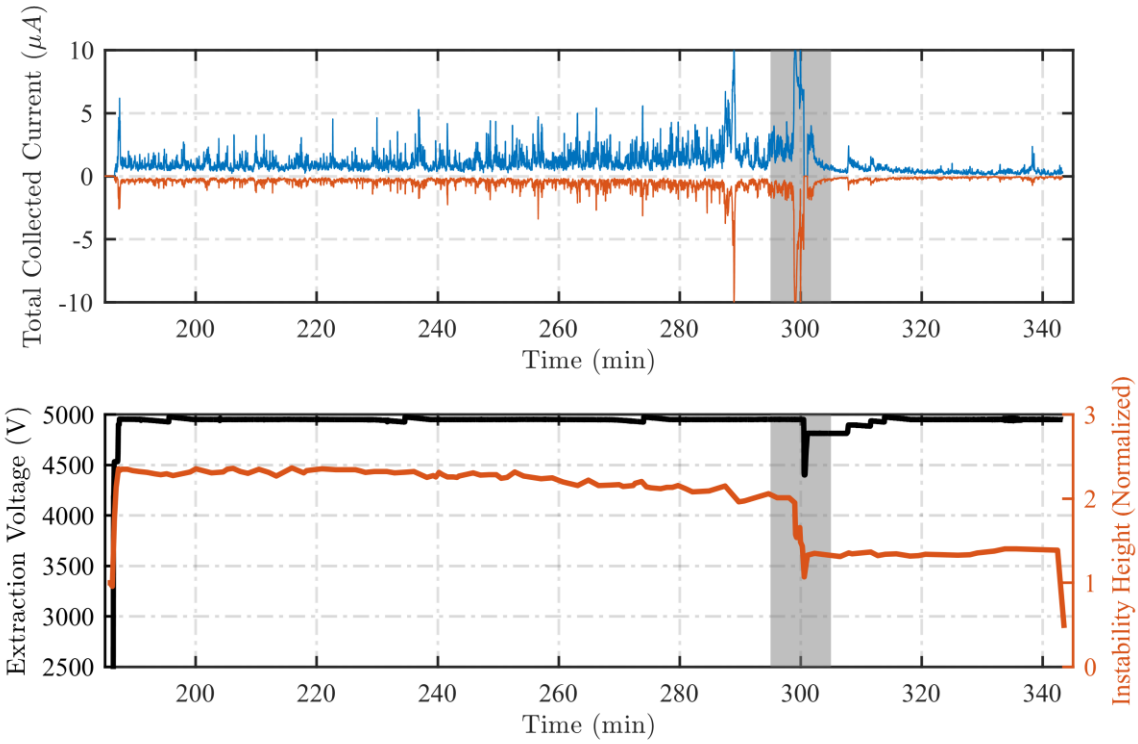

Figure 18: Constant voltage emission test with 1-magnet.

During this emission mode, the emitter appeared to be in a relatively high current, low mass flow rate regime. It is possible that the emitter was operating in a regime which yielded a larger percentage of ion emission or a regime

which yielded relatively smaller droplets. Recall from Eq. (4), the charge to mass ratio of a droplet at the Rayleigh limit is proportional to $r^{-3/2}$.

At approximately 300 minutes into the test case presented in Figure 18, the source experienced a sudden and rapid increase in the emission current. Due to the saturation of the current sensors, the extraction voltage was shut-off in response to this event then increased again to resume emission. Snapshots of the emitter leading up to and after this event are presented in Figure 19. It is a possibility that the constituents of the spray are not equivalent to the nano-particle to carrier fluid ratio. The result would yield a buildup of nanoparticles near the emission site which would provide hydraulic impedance to the flow. The hydraulic impedance is a critical factor in controlling the emission mode of an electrospray source, as discussed by Krpoun et. al.[23]

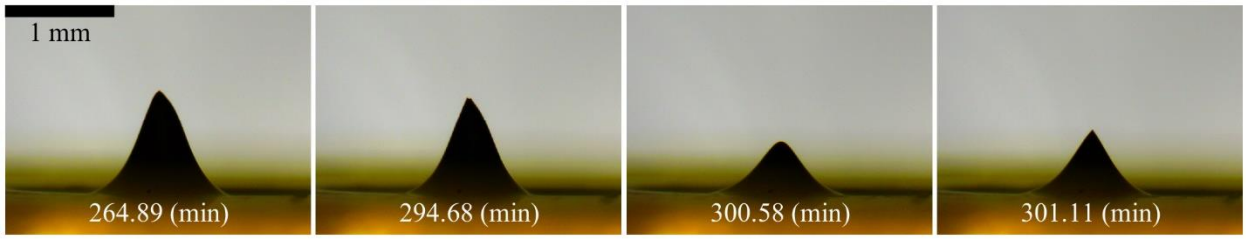

Figure 19: Ferrofluid interface during select moment of constant voltage emission test. Prior to 300 minutes, the fluid apex would vary between 1 and 2 emission sites. At approximately 115 minutes, a mass of fluid was ejected from the apex of the emission source shifting the emitter into a different emission mode.

IV.Conclusion

A model was developed to analyze the magnetic and electric stresses that would exist near the apex of a Taylor cone during electrospray emission. The Kelvin force, which becomes present when emitting magnetic nanoparticles, and the $q\vec{v}\times\vec{B}$ term in the Lorentz force were found to be trivial in comparison with the electrostatic forces. Long duration emission tests were then conducted of an ionic liquid ferrofluid electrospray source, during which angular divergence measurements were continuously taken. These measurements show that the angle at which the collected current drops to zero is about 20° for both field strengths investigated. During extended testing, multiple emission modes were observed. It is hypothesized that the emission modes may depend on the buildup of nanoparticles at the fluid apex – a process which merits further investigation.

Acknowledgments

The authors would like to thank the Air Force Office of Scientific Research for their support funding this research.

References

1. Hawket, B., and Sabouri, H. "Saturatization Magnetization for ILFF Samples." 9/21/16, 2016.
2. King, L. B., Meyer, E., Hopkins, M. A., Hawkett, B. S., and Jain, N. "Self-Assembling Array of Magnetoelectrostatic Jets from the Surface of a Superparamagnetic Ionic Liquid," *Langmuir* Vol. 30, No. 47, 2014, pp. 14143-14150.
3. Jain, N., Zhang, X., Hawkett, B. S., and Warr, G. G. "Stable and water-tolerant ionic liquid ferrofluids," *ACS Applied Materials & Interfaces* Vol. 3, No. 3, 2011, pp. 662-667.
4. Terhune, K. J., King, L. B., Prince, B. D., Jain, N., and Hawkett, B. S. "The effects of magnetic surface stress on electrospray of an ionic liquid ferrofluid," *52nd AIAA/SAE/ASEE Joint Propulsion Conference*. 2016, p. 4549.
5. Meyer IV, E. J., and King, L. B. "Electrospray from an Ionic Liquid Ferrofluid utilizing the Rosensweig Instability." 49th AIAA/ASME/SAE/ASEE Joint Propulsion Conferene & Exhibit, Paper No. AIAA-2013-3823, 14-17 July 2013, San Jose, CA, 2013.
6. IV, E. J. M., King, L. B., Jain, N., and Hawkett, B. S. "Ionic liquid ferrofluid electrospray with EMIM-NTf2 and ferrofluid mode studies with FerroTec EFH-1 in a non-uniform magnetic field," 2013.
7. Terhune, K. J., King, L. B., Hause, M. L., Prince, B. D., Jain, N., and Hawkett, B. S. "Species measurements in the beam of an ionic liquid ferrofluid electrospray source," *50th AIAA/ASME/SAE/ASEE Joint Propulsion Conference & Exhibit*. AIAA, Cleveland, OH, 2014.
8. Jackson, B. A., Terhune, K. J., and King, L. B. "Ionic liquid ferrofluid interface deformation and spray onset under electric and magnetic stresses," *Physics of Fluids* Vol. 29, No. 6, 2017, p. 064105. doi: 10.1063/1.4985141
9. Gamero-Castano, M., and Fernandez De La Mora, J. "Direct measurement of ion evaporation kinetics from electrified liquid surfaces," *The Journal of Chemical Physics* Vol. 113, No. 2, 2000, pp. 815-832.

10. Rosensweig, R. E. *Ferrohydrodynamics*: Courier Dover Publications, 1997.
11. Jaworek, A. "Electrospray droplet sources for thin film deposition," *Journal of Materials Science* Vol. 42, No. 1, 2007, pp. 266-297.
12. Krpoun, R., and Shea, H. R. "A method to determine the onset voltage of single and arrays of electrospray emitters," *Journal of Applied Physics* Vol. 104, No. 6, 2008, p. 064511.
13. Wang, Y., Tan, M. K., Go, D. B., and Chang, H.-C. "Electrospray cone-jet breakup and droplet production for electrolyte solutions," *EPL (Europhysics Letters)* Vol. 99, No. 6, 2012, p. 64003.
14. Terhune, K. J., King, L. B., Prince, B. D., Jain, N., and Hawkett, B. S. "Species measurements in the beam of an ionic liquid ferrofluid capillary electrospray source under magnetic stress," *52nd AIAA/SAE/ASEE Joint Propulsion Conference*. 2016, p. 4550.
15. Lozano, P., and Martínez-Sánchez, M. "Studies on the ion-droplet mixed regime in colloid thrusters," *Department of Aeronautics and Astronautics, Massachusetts Institute of Technology*, 2003.
16. Jackson, B. A., King, L. B., Jain, N., and Hawkett, B. S. "Characterization of an Ionic Liquid Ferrofluid Electrospray Emission Pattern," *50th AIAA/ASME/SAE/ASEE Joint Propulsion Conference & Exhibit*. AIAA, Cleveland, OH, 2014.
17. Chiu, Y.-H., Gaeta, G., Levandier, D., Dressler, R., and Boatz, J. "Vacuum electrospray ionization study of the ionic liquid,[Emim][Im]," *International Journal of Mass Spectrometry* Vol. 265, No. 2, 2007, pp. 146-158.
18. Courtney, D. G., Dandavino, S., and Shea, H. "Comparing Direct and Indirect Thrust Measurements from Passively Fed Ionic Electrospray Thrusters," *Journal of Propulsion and Power*, 2015.
19. Gamero-Castaño, M. "Characterization of the electrosprays of 1-ethyl-3-methylimidazolium bis (trifluoromethylsulfonyl) imide in vacuum," *Physics of Fluids (1994-present)* Vol. 20, No. 3, 2008, p. 032103.
20. Gamero-Castano, M. "The structure of electrospray beams in vacuum," *Journal of Fluid Mechanics* Vol. 604, 2008, pp. 339-368.
21. Morris, T., Malardier-Jugroot, C., and Jugroot, M. "Characterization of electrospray beams for micro-spacecraft electric propulsion applications," *Journal of Electrostatics* Vol. 71, No. 5, 2013, pp. 931-938.
22. Jones, D. "uCurrent Original." Vol. 2017, 2010, p. https://www.eevblog.com/projects/ucurrentoriginal/.
23. Krpoun, R., Smith, K. L., Stark, J. P. W., and Shea, H. R. "Tailoring the hydraulic impedance of out-of-plane micromachined electrospray sources with integrated electrodes," *Applied Physics Letters* Vol. 94, No. 16, 2009, p. 163502.
doi: 10.1063/1.3117191